FRONTIERS OF PHYSICS

RESEARCH ARTICLE
Volume 18 / Issue 5 / 52302 / 2023

Epitaxial growth of 2D gallium selenide flakes for strong nonlinear optical response and visible-light photodetection

Mengting Song[1,#], Nan An[1,#], Yuke Zou[1], Yue Zhang[1], Wenjuan Huang[1,2,†], Huayi Hou[1], Xiangbai Chen[1,‡]

1 Hubei Key Laboratory of Optical Information and Pattern Recognition, Wuhan Institute of Technology, Wuhan 430205, China
2 State Key Laboratory of Materials Processing and Die & Mould Technology, School of Materials Science and Engineering, Huazhong University of Science and Technology, Wuhan 430074, China
Corresponding authors. E-mail: †wjhuang@wit.edu.cn, ‡xchen@wit.edu.cn
#These two authors contributed equally to the work.
Received August 11, 2022; accepted November 2, 2022

ABSTRACT

As an emerging group III–VI semiconductor two-dimensional (2D) material, gallium selenide (GaSe) has attracted much attention due to its excellent optical and electrical properties. In this work, high-quality epitaxial growth of few-layer GaSe nanoflakes with different thickness is achieved via chemical vapor deposition (CVD) method. Due to the non-centrosymmetric structure, the grown GaSe nanoflakes exhibits excellent second harmonic generation (SHG). In addition, the constructed GaSe nanoflake-based photodetector exhibits stable and fast response under visible light excitation, with a rise time of 6 ms and decay time of 10 ms. These achievements clearly demonstrate the possibility of using GaSe nanoflake in the applications of nonlinear optics and (opto)-electronics.

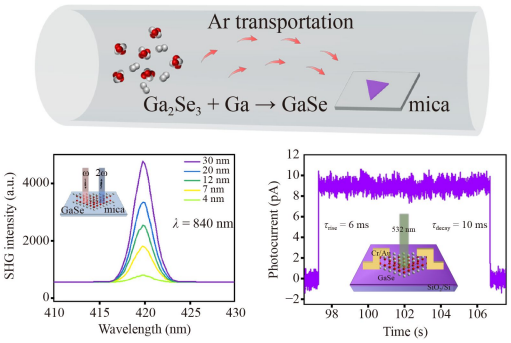

Keywords 2D materials, gallium selenide, second harmonic generation, chemical vapor deposition, photodetector

1 Introduction

Two-dimensional (2D) materials have attracted great attention due to their excellent electronic and optoelectronic properties [1, 2]. So far, the most widely studied 2D semiconductor materials are graphene [3–6], black phosphorus [7–10], and transition metal dichalcogenides such as MX_2 (M = Mo, W; X = S, Se) [11–14]. The in-plane chemical bonds of 2D materials are very strong, and the interaction between layers is relatively weak, generally van der Waals interaction [15]. Different 2D materials can be stacked in a horizontal or vertical manner to form a 2D heterostructure in a certain sequence by artificial means to realize a variety of different functional devices [16, 17]. Whether it is a single 2D material or its heterostructure, its energy band structure and optical properties have significant layer number dependence [18–22].

Gallium selenide (GaSe) is a 2D layered material with a unique four-layer Se–Ga–Ga–Se structure and the thickness of a single layer of GaSe is 0.8 nm [23]. The band gap of GaSe increases as the number of layers

*Special Topic: Two-dimensional Materials for Optoelectronics (Eds.: Tianyou Zhai & Xing Zhou).

Higher Education Press

https://doi.org/10.1007/s11467-023-1277-3

decreases. When the number of atomic layers of the GaSe crystal is less than 7, it changes from a direct band gap semiconductor to an indirect band gap semiconductor [24]. It is worth noting that GaSe is a p-type 2D semiconductor [25], which can be combined with other n-type 2D semiconductors to form a p-n junction with unidirectional conductivity. Due to its unique electronic structure, GaSe can achieve power output in the terahertz band, and has a wide range of applications in non-linear optics, optoelectronic devices and other fields [26–28].

So far, many methods have been tried to obtain high-quality 2D GaSe, including mechanical exfoliation [29], pulsed laser deposition [30, 31], molecular beam epitaxy [32–34], electrochemical deposition [35], vapor–liquid–solid [36], and chemical vapor deposition (CVD) method [26, 37–44]. Among all these methods, the CVD method is the most effective method to achieve high-quality 2D GaSe growth. Here, we report a facile method for growing GaSe nanoflakes with different thicknesses via CVD method. The synthesized GaSe nanoflakes showed a triangular morphology with an average size of ~10 μm. Moreover, thickness-dependent optical properties of GaSe nanoflakes were investigated by Raman, photoluminescence (PL) and second harmonic generation (SHG). In addition, GaSe nanoflake-based photodetector was constructed to study the optoelectronic properties of synthesized GaSe nanoflake, which exhibited a stable and fast response under visible light illumination.

2 Experimental section

Synthesis of GaSe samples. The growth of GaSe samples was carried out in a single temperature zone tube furnace equipped with a quartz tube. Ga_2Se_3 powder (Alfa, purity 99.99%) and Ga (MACKLIN, purity 99.999%) were placed in the center of the heating zone. Mica substrate were placed at the downstream of the heating zone. Prior to heating, the whole system was purged by Ar for ~30 minutes to remove the air in the tube. The furnace was heated up to 880–920 °C at a rate of 25 °C/min with 35–45 sccm Ar and then maintained for 10 min for the growth of GaSe. After the annealing, the furnace was naturally cooled to room temperature. The pressure for the growth of GaSe was under ambient pressure.

Transfer of CVD-grown GaSe nanoflakes. The as-grown GaSe sample on mica substrate was then transferred onto an SiO_2/Si substrate. First, the GaSe sample on mica substrate was spin-coated with PMMA at 4000 rpm for 1min, and then baked at 155 °C for 5 min in order to enhance the adhesion force between PMMA and GaSe samples. Then, PPC (20 wt%, dissolved in anisole) was spin-coated on the top of PMMA film at 2000 rpm for 1 min, followed by baking at 110 °C for 10 min. Afterwards, the PPC/PMMA polymer carrying GaSe samples was peeled off slowly from the mica substrate by tweezers. Next, the PPC/PMMA polymer was placed on the SiO_2/Si (300 nm) substrate and isopropanol was added dropwise to make it adsorb on the surface of the substrate. The PPC/PMMA polymer was uniformly attached to the surface of the SiO_2/Si substrate by baking at 90 °C for 15 min. The TEM samples were prepared by the same method, except that the SiO_2/Si substrate was replaced by a microgrid.

Characterizations. The as-prepared products were further characterized by optical microscopy (Olympus BX41 microscope), atomic force microscope (Dimension Icon, BRUKER), and transmission electron microscope (TEM, JEM-2100, JEOL). Raman, PL spectra of GaSe samples with different thicknesses were recorded in a confocal Raman spectroscopy (Alpha 300RS+, WITec) using a 532 nm laser as the excitation source. For SHG measurement, we use an Alpha 300RS+ Raman spectroscopy by introducing a femtosecond laser as the excitation source. A mode-locked Ti: sapphire was used to generate a continuously adjustable laser wavelength from 800 nm to 1080 nm with pluse duration of 140 fs and repetition rate of 80 MHZ and filtered into optical parametric oscillator (Chameleon Compact OPO-Vis). The output laser beam was focused on the sample with a spot size of about 1.8 μm by 100× objective. For SHG polarization measurement, the collected parallel-polarized SHG signal was sent through a linear polarized analyzer by rotating the sample with a step of 15 ° relative to the fixed light polarization. More details about the SHG test setup were described in previous work [45]. All experiments were performed at room temperature.

Device fabrication and measurement. The devices were fabricated by transferring GaSe nanoflakes onto SiO_2/Si (300 nm) substrate. The electrodes were patterned on the samples by electron beam lithography (Quanta 650 SEM, FEI and ELPHY Plus, Raith GmbH), and then Cr/Au (10 nm/50 nm) layers were deposited on the GaSe nanoflakes with thermally evaporated deposition (Nexdap, Angstrom Engineering). The photodetector measurements were carried out by a semiconductor characterization system (B1500A, Agilent) under the illumination of 532 nm light pulse with area of light spot of 0.44 cm^2 in a probe station (CRX-6.5K, Lake Shore). All the measurements were performed in air and at room temperature.

3 Results and discussion

In this study, the GaSe samples were grown on mica substrates via a vapor phase growth process in a tube furnace [Fig. 1(a)]. Growth kinetics depend on the Ga/Se ratio of the precursor in the local growth zone, but

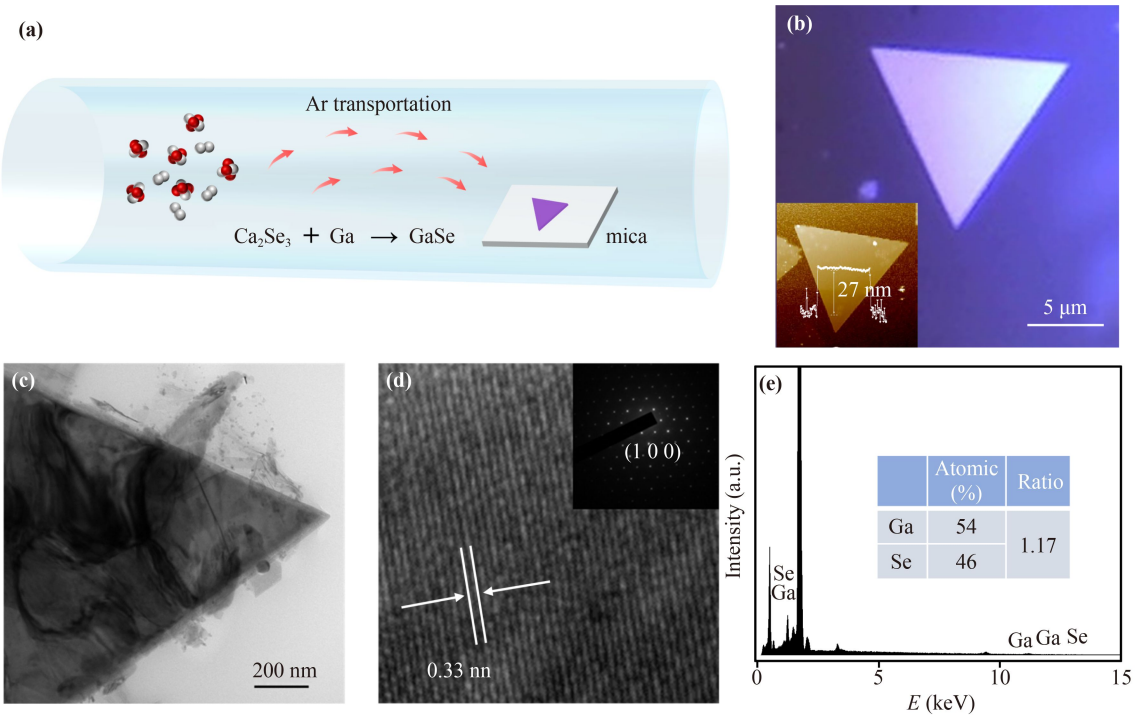

Fig. 1 Synthesis of GaSe nanoflakes by CVD method. **(a)** Schematic diagram of 2D GaSe nanoflakes growth by a CVD system. **(b)** Optical image of GaSe nanoflake. Inset: AFM image of GaSe nanoflake. **(c)** TEM image of GaSe nanoflake. **(d)** HRTEM image of GaSe nanoflake. Inset: Corresponding SAED pattern. **(e)** EDX spectrum of GaSe nanoflake. Inset: Atomic ratio of Ga/Se.

the Ga/Se ratio at different positions is usually not constant due to the weight difference between Ga and Se. Therefore, by deviating the Ga/Se ratio from the theoretical ratio of 1:1 throughout the growth region, a uniform morphology of GaSe nanoflakes can be obtained, which is also manifested in the vapor phase growth of other 2D materials [38]. The growth of GaSe nanoflakes can be carried out at a mass ratio of Ga_2Se_3:Ga = 1:1.1. Figure 1(b) shows the optical images of GaSe nanoflake with size of ~10 μm. The thickness of a typical GaSe nanoflake mica substrate was determined to be ~27 nm by AFM measurements [inset of Fig. 1(b)]. Figure 1(c) shows a TEM image of a typical GaSe nanoflake, indicating the standard triangular morphology of as-synthesized GaSe nanoflakes. The high-resolution TEM (HRTEM) image of GaSe nanoflake is shown in Fig. 1(d). The lattice spacing of 0.33 nm is in accordance with the (100) interplanar distance of GaSe (PDF#01-078-2499 [46]). The corresponding selected area electron diffraction (SAED) pattern is presented in the inset of Fig.1(d), showing single crystalline of as-synthesized GaSe nanoflakes. From the EDS spectrum of the GaSe nanoflake as shown in Fig. 1(e), the signals of Ga and Se can be detected with atomic ratio of Ga/Se of 1.17 [inset of Fig. 1(e)], approximately equal to the theoretical stoichiometric value of GaSe.

Figure 2(a) shows the Raman spectra of 2D GaSe nanoflakes with different thicknesses with a laser excitation of 532 nm. For a GaSe nanoflakes with thickness of 6 nm, Raman characteristic peaks of GaSe and mica substrate located at 197 and 270 cm^{-1} can be observed. With the increase of thickness of GaSe nanoflake, the characteristic peak intensity of GaSe increases, while the Raman peak of mica substrate gradually weakens until disappears. Three distinct characteristic Raman peaks located at 132, 213, and 308 cm^{-1} are clearly observed, assigned to the A^1_{1g}, E^1_{2g}, A^2_{1g} modes of GaSe, respectively [23]. As the thickness increases, the Raman characteristic peaks of GaSe shift to the lower wavenumber direction. This is because with the increase of the number of layers, the vibrational activity of atoms in the layer is hindered, thereby reducing its vibrational energy, resulting in a red shift of the Raman peak positions corresponding to the three vibrational modes [47]. PL spectroscopy was employed to evaluate the optical properties of GaSe nanoflakes, as seen in Fig. 2(b). Under the excitation of 532 nm wavelength, the GaSe nanoflake with thickness of 30 nm exhibits an obvious peak at ~629 nm (1.97 eV), which is similar to the GaSe reported [39], corresponding to the bandgap of GaSe [30]. A weak PL peak at ~606 nm (2.05 eV) can be observed in a thin GaSe flake with thickness of ~4 nm, which may be due to the transition from direct to indirect bandgap when the thickness is reduced to few-layer [24]. As the thickness increases, the PL intensity of GaSe is found to increase and a broad peak from 650 nm to 800 nm assigned to the underneath

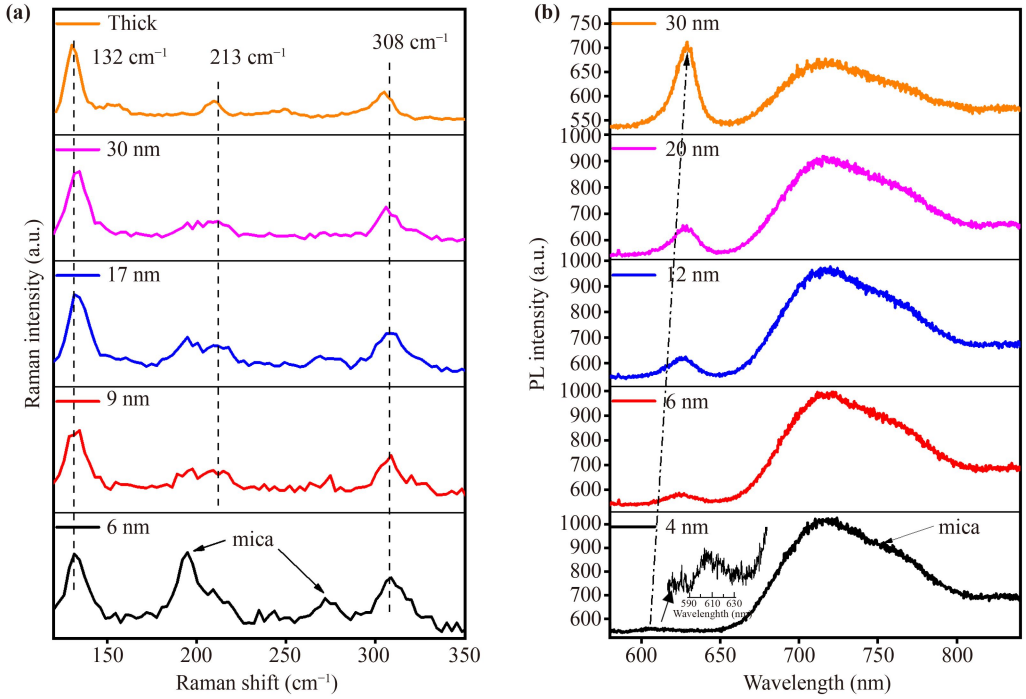

Fig. 2 **(a)** Thickness-dependent Raman spectra of GaSe nanoflakes. **(b)** Thickness-dependent PL spectra of GaSe nanoflakes.

mica substrate is observed to decrease. Owing to the strong quantum confinement effects [48], a red-shifted variation can be observed as the thickness increases.

The non-centrosymmetric structure is the key factor of second harmonic generation (SHG)[49]. Figure 3(a) shows the SHG signal at 400 nm wavelength under excitation at 800 nm wavelength, and its intensity increases with laser power, which shows a linear dependence with a slope of 2.03 by power-law fitting [shown in Fig. 3(b)]. Compared with transition metal chalcogenides (monolayer has a non-centrosymmetric structure), GaSe maintains a non-centrosymmetric structure at all thicknesses, so its SHG signal intensity increases with its thickness [shown in Fig. 3(c)]. The key that must be considered in nonlinear applications is the spectral range of the material that can generate SHG signals. Figure 3(d) shows the SHG generated by the excitation of GaSe nanoflake within the different wavelength range of 800–1080 nm. In order to study the crystal symmetry of a single GaSe nanoflake, we tested the polarization second harmonic generation by rotating the sample during the test, and collecting parallel polarized light. As shown in Fig. 3(e), as the azimuth changes, we can observe that the SHG intensity exhibits a 6-axis symmetry pattern. Figure 3(f) shows the SHG mapping of a single triangular-shaped GaSe nanoflake under excitation of 840 nm. SHG results indicate that the synthesized GaSe exhibits excellent nonlinear optical properties due to its non-centrosymmetric structure.

To explore the optoelectronic properties of the GaSe nanoflakes, GaSe-based photodetectors were fabricated on SiO_2/Si substrate. Figure 4(a) shows the schematic image of the photodetector. Fig. 4(b) shows the current–voltage (I–V) curve measured of the GaSe-based photodetector under 532 nm laser excitation and in the dark, respectively. It is found that the device exhibited a Schottky contact between the Cr/Au electrodes and the GaSe nanoflake. Under excitation of 532 nm, the optimal photoresponsivity (R_λ) is 2.7 mA/W. The external quantum efficiency (EQE) and detectivity (D^*) of the GaSe-based photodetector at a wavelength of 532 nm is 0.63 % and 8.7 × 10^7 Jones, respectively. Calculated by the relations of $EQE = hcR_\lambda/e\lambda$ and $D^* = R_\lambda S^{1/2}/(2eI_{\text{dark}})^{1/2}$, where the parameters h, c, λ, e, and I_{dark} are Plank's constant, light velocity, excited wavelength, elementary electronic charge and dark current, respectively. Figure 4(c) shows that the GaSe-based photodetector exhibits a repeatable and stable response to incident light. Photo-response time is another critical parameter used to judge device performance. We investigated the time-resolved photo-response of the device by switching the laser on and off. Figure 4(d) displays a single cycle response of laser on and off. The photodetector shows a fast response rate of 6 ms for the rise and 10 ms for the decay times. The trend of the photocurrent changes with time under different illumination intensities of 9.93–41.65 mW/cm^2 for the GaSe-based photodetector is shown in Fig. 4(e). It can be seen from Fig. 4(e) that as the optical power density increases, its photocurrent also increases. The relationship between light intensity and

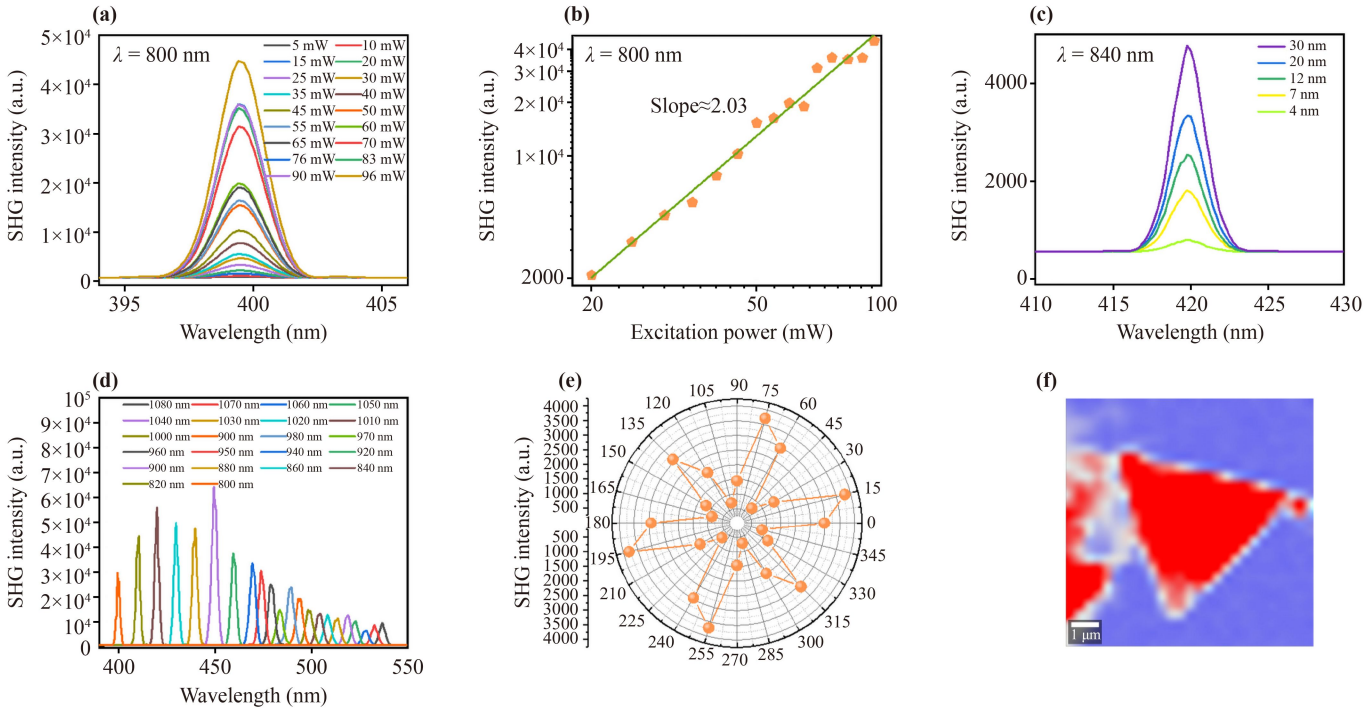

Fig. 3 The second harmonic generation (SHG) test of 2D GaSe nanoflake: **(a)** SHG intensity of GaSe flake with different excitation power and **(b)** the corresponding linear fitting. **(c)** SHG intensity of GaSe nanoflakes with different thicknesses. **(d)** Wavelength dependence of SHG intensity from 800 to 1080 nm. **(e)** SHG polarization test of 2D GaSe nanoflake, rotating the sample angle θ at a step of 15°, showing a 6-axis rotating scale; **(f)** SHG mapping of a single GaSe nanoflake.

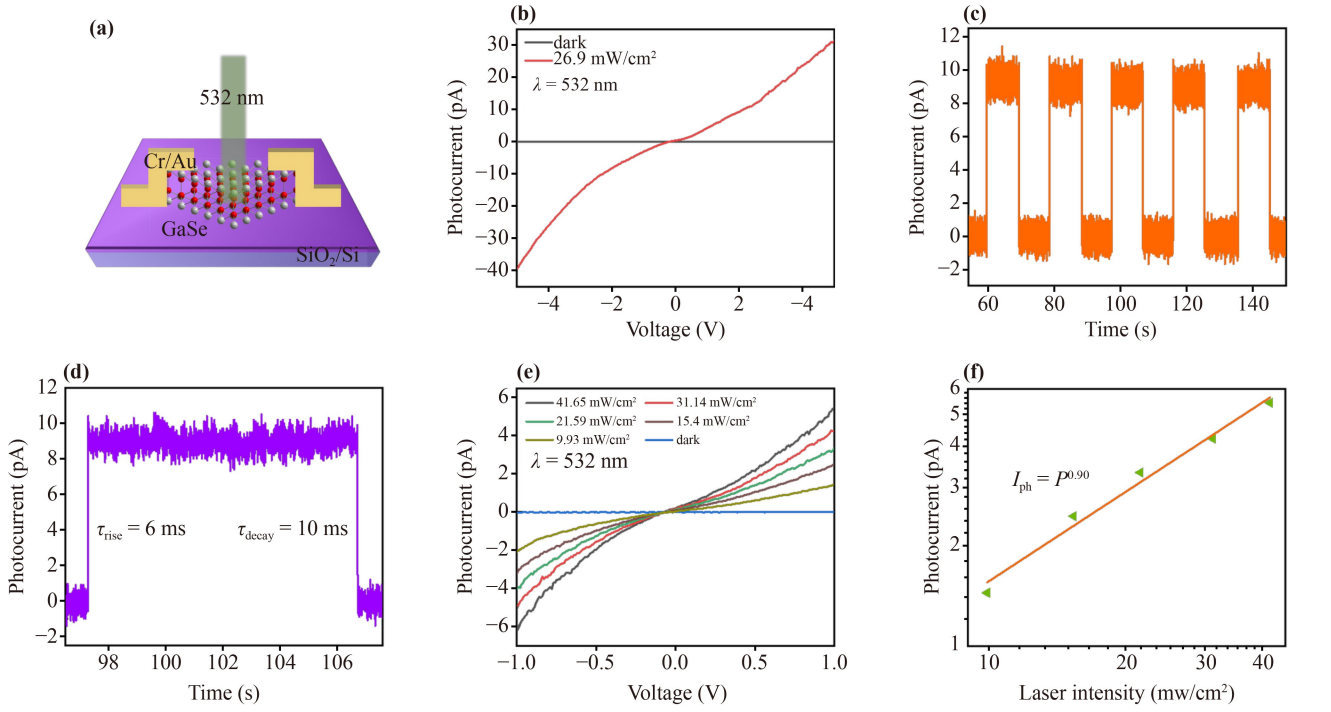

Fig. 4 **(a)** Schematic image of the photodetector. **(b)** *I*–*V* characteristics of the device in the dark and under light illumination with wavelength at 532 nm (V_{bias} = 5 V). **(c)** Time-resolved photoresponse of the device at 532 nm (V_{bias} = 2 V). **(d)** Rise and decay curve measured under 532 nm excitation at V_{bias} = 2 V. **(e)** Photocurrent as a function of illumination intensity at V_{bias} = 1 V under 532 nm excitation. (f) The corresponding fitting curve of photocurrent versus incident light intensities by the power law.

Table 1 Comparison of the key parameters of our device to the reported 2D materials and the other structures of GaSe-based photodetectors.

Device	Fabrication methods	R_λ (mA·W^{-1})	EQE (%)	D^* (Jones)	Rise time (ms)	Decay time (ms)	Ref.
Graphene	ME	1.0	6–16	–	–	–	[52]
$MoSe_2$	CVD	13	–	–	~60	~60	[53]
WS_2	CVD	7.3×10^3	1814	–	5	5	[13]
$ReSe_2$	CVD	2.98×10^3	458	–	5.47×10^3	8.41×10^3	[54]
HfS_2	CVD	2.8	–	–	55	55	[55]
InSe	CVD	1.5×10^3	230	3.1×10^8	500	800	[56]
In_2Se_3	MBE	3	0.67	10^9	≈7	≈7	[57]
GaS	CVD	50	23	–	–	–	[58]
GaSe	VPM	17	5.2	–	–	–	[59]
GaSe	CVD	2.7	0.63	8.7×10^7	6	10	This work

Note. ME: Mechanical exfoliation; MBE: Molecular beam epitaxy; VPM: Vapor phase mass transport.

photocurrent can be fitted by the Power Law formula of $I_{ph} \propto P^\theta$ [50, 51] (where I_{ph} is the light response current, P is the light power density, and θ is an index associated with the light response at a certain light intensity). As shown in Fig. 4(f), the photocurrent increases linearly with the increase of optical power density, and its θ is 0.90, which indicates that the synthesized GaSe-based photodetector has excellent photocurrent capability. Some reported device performance data are summarized in Table 1.

4 Conclusion

In conclusion, we achieved the synthesis of GaSe nanoflakes with different thicknesses via CVD method. GaSe nanoflakes with triangle morphology can be obtained under different Ga/Se ratios by adjusting the ratio of two source species. A series of characterizations showed that the synthesized GaSe samples crystallized well and exhibited excellent performance. The layer-dependent optical properties of GaSe nanosheets were investigated by Raman, PL and SHG characterization. Simultaneously, SHG characterization shows that the synthesized GaSe samples exhibit excellent nonlinear optical properties due to their non-centrosymmetric structure. Under visible light illumination, the photodetectors based on GaSe nanoflakes exhibit stable and fast photoresponse with a rise time of 6 ms and decay time of 10 ms. This provides a reference for the preparation of 2D materials and the possibility of using GaSe nanoflakes for potential applications in nonlinear optics and (opto)-electronics.

Declaration of competing interest The authors declare that they have no known competing financial interests or personal relationships that could have appeared to influence the work reported in this paper.

CRediT authorship contribution statement Mengting Song: Investigation, Experiment, Writing, Validation. Nan An: Co-first authors, Investigation, Experiment, Validation. Yuke Zou: Investigation, Experiment. Yue Zhang: Investigation, Software. Wenjuan Huang: Methodology, Experiment, Supervision. Huayi Hou: Validation. Xiangbai Chen: Writing-reviewing & editing, Supervision.

Acknowledgements This work was supported by the National Natural Science Foundation of China (Grant Nos. 51902227 and 11574241) and the Open Project of State Key Laboratory of Materials Processing and Die & Mould Technology, Huazhong University of Science and Technology, China (Grant No. P2020-021).

References

1. J. L. Zhao, D. Ma, C. Wang, Z. N. Guo, B. Zhang, J. Q. Li, G. H. Nie, N. Xie, and H. Zhang, Recent advances in anisotropic two-dimensional materials and device applications, *Nano Res.* 14(4), 897 (2021)
2. A. Zavabeti, A. Jannat, L. Zhong, A. A. Haidry, Z. Yao, and J. Z. Ou, Two-dimensional materials in large-areas: Synthesis, properties and applications, *Nano-Micro Lett.* 12(1), 66 (2020)
3. A. Alexeev, M. Barnes, V. K. Nagareddy, M. Craciun, and D. Wright, A simple process for the fabrication of large-area CVD graphene based devices via selective *in situ* functionalization and patterning, *2D Mater.* 4, 011010 (2016)
4. N. E. Safie, M. A. Azam, M. F. A. Aziz, and M. Ismail, Recent progress of graphene-based materials for efficient charge transfer and device performance stability in perovskite solar cells, *Int. J. Energy Res.* 45(2), 1347 (2021)
5. A. K. Geim, Graphene: Status and prospects, *Science* 324(5934), 1530 (2009)
6. L. Huang, Q. H. Chang, G. L. Guo, Y. Liu, Y. Q. Xie, T. Wang, B. Ling, and H. F. Yang, Synthesis of high-quality graphene films on nickel foils by rapid thermal chemical vapor deposition, *Carbon* 50(2), 551 (2012)
7. F. N. Xia, H. Wang, and Y. C. Jia, Rediscovering black phosphorus as an anisotropic layered material for opto-electronics and electronics, *Nat. Commun.* 5(1), 4458 (2014)

8. Y. Chen, G. B. Jiang, S. Q. Chen, Z. N. Guo, X. F. Yu, C. J. Zhao, H. Zhang, Q. L. Bao, S. C. Wen, D. Y. Tang, and D. Y. Fan, Mechanically exfoliated black phosphorus as a new saturable absorber for both *Q*-switching and mode-locking laser operation, *Opt. Express* 23(10), 12823 (2015)
9. M. Buscema, D. J. Groenendijk, S. I. Blanter, G. A. Steele, H. S. van der Zant, and A. Castellanos-Gomez, Fast and broadband photoresponse of few-layer black phosphorus field-effect transistors, *Nano Lett.* 14(6), 3347 (2014)
10. L. K. Li, Y. J. Yu, G. J. Ye, Q. Q. Ge, X. D. Ou, H. Wu, D. L. Feng, X. H. Chen, and Y. B. Zhang, Black phosphorus field-effect transistors, *Nat. Nanotechnol.* 9(5), 372 (2014)
11. A. Singh, M. Moun, M. Sharma, A. Barman, A. Kumar Kapoor, and R. Singh, NaCl-assisted substrate dependent 2D planar nucleated growth of MoS_2, *Appl. Surf. Sci.* 538, 148201 (2021)
12. W. Wang, H. Shu, J. Wang, Y. Cheng, P. Liang, and X. Chen, Defect passivation and photoluminescence enhancement of monolayer MoS_2 crystals through sodium halide-assisted chemical vapor deposition growth, *ACS Appl. Mater. Interfaces* 12(8), 9563 (2020)
13. Y. Chen, Growth of a large, single-crystalline WS_2 monolayer for high-performance photodetectors by chemical vapor deposition, *Micromachines (Basel)* 12(2), 137 (2021)
14. Z. Wang, Y. Xie, H. Wang, R. Wu, T. Nan, Y. Zhan, J. Sun, T. Jiang, Y. Zhao, Y. Lei, M. Yang, W. Wang, Q. Zhu, X. Ma, and Y. Hao, NaCl-assisted one-step growth of MoS_2-WS_2 in-plane heterostructures, *Nanotechnology* 28(32), 325602 (2017)
15. M. Chhowalla, H. S. Shin, G. Eda, L. J. Li, K. P. Loh, and H. Zhang, The chemistry of two-dimensional layered transition metal dichalcogenide nanosheets, *Nat. Chem.* 5(4), 263 (2013)
16. K. S. Novoselov, A. Mishchenko, A. Carvalho, and A. H. Castro Neto, 2D materials and van der Waals heterostructures, *Science* 353(6298), aac9439 (2016)
17. A. K. Geim and I. V. Grigorieva, Van der Waals heterostructures, *Nature* 499(7459), 419 (2013)
18. J. F. Li, S. Kolekar, M. Ghorbani-Asl, T. Lehnert, J. Biskupek, U. Kaiser, A. V. Krasheninnikov, and M. Batzill, Layer-dependent band gaps of platinum dichalcogenides, *ACS Nano* 15(8), 13249 (2021)
19. J. W. Jiang, H. Tang, B. S. Wang, and Z. B. Su, Raman and infrared properties and layer dependence of the phonon dispersions in multilayered graphene, *Phys. Rev. B* 77(23), 235421 (2008)
20. M. Tamulewicz, J. Kutrowska-Girzycka, K. Gajewski, J. Serafinczuk, A. Sierakowski, J. Jadczak, L. Bryja, and T. P. Gotszalk, Layer number dependence of the work function and optical properties of single and few layers MoS_2: Effect of substrate, *Nanotechnology* 30(24), 245708 (2019)
21. X. L. Li, W. P. Han, J. B. Wu, X. R. Qiao, J. Zhang, and P. H. Tan, Layer-number-dependent optical properties of 2D materials and their application for thickness determination, *Adv. Funct. Mater.* 27(19), 1604468 (2017)
22. R. He, J. van Baren, J. Yan, X. Xi, Z. Ye, G. Ye, I. H. Lu, S. M. Leong, and C. H. Lui, Interlayer breathing and shear modes in $NbSe_2$ atomic layers, *2D Mater.* 3(3), 031008 (2016)
23. L. Quan, Y. Q. Song, Y. Lin, G. H. Zhang, Y. M. Dai, Y. K. Wu, K. Jin, H. Y. Ding, N. Pan, Y. Luo, and X. P. Wang, The Raman enhancement effect on a thin GaSe flake and its thickness dependence, *J. Mater. Chem. C* 3(42), 11129 (2015)
24. X. F. Li, M. W. Lin, A. A. Puretzky, J. C. Idrobo, C. Ma, M. F. Chi, M. Yoon, C. M. Rouleau, I. I. Kravchenko, D. B. Geohegan, and K. Xiao, Controlled vapor phase growth of single crystalline, two-dimensional GaSe crystals with high photoresponse, *Sci. Rep.* 4(1), 5497 (2014)
25. V. V. Capozzi and M. Montagna, Optical spectroscopy of extrinsic recombinations in gallium selenide, *Phys. Rev. B* 40(5), 3182 (1989)
26. Z. X. Zou, J. W. Liang, X. H. Zhang, C. Ma, P. Xu, X. Yang, Z. X. Zeng, X. X. Sun, C. G. Zhu, D. L. Liang, X. J. Zhuang, D. Li, and A. L. Pan, Liquid–metal-assisted growth of vertical GaSe/MoS_2 p–n heterojunctions for sensitive self-driven photodetectors, *ACS Nano* 15(6), 10039 (2021)
27. Y. Tang, K. C. Mandal, J. A. McGuire, and C. W. Lai, Layer- and frequency-dependent second harmonic generation in reflection from GaSe atomic crystals, *Phys. Rev. B* 94(12), 125302 (2016)
28. D. X. Yan, Y. Y. Wang, D. G. Xu, P. X. Liu, C. Yan, J. Shi, H. X. Liu, Y. X. He, L. H. Tang, J. C. Feng, J. Q. Guo, W. Shi, K. Zhong, Y. H. Tsang, and J. Q. Yao, High-average-power, high-repetition-rate tunable terahertz difference frequency generation with GaSe crystal pumped by 2 μm dual-wavelength intracavity KTP optical parametric oscillator, *Photon. Res.* 5(2), 82 (2017)
29. H. C. Hsu, G. M. Hsu, Y. Lai, Z. C. Feng, S. Y. Tseng, A. Lundskog, U. Forsberg, E. Janzén, K. H. Chen, and L. C. Chen, Polarized and diameter-dependent Raman scattering from individual aluminum nitride nanowires: The antenna and cavity effects, *Appl. Phys. Lett.* 101(12), 121902 (2012)
30. S. H. Lee, Y. Hsu, H. Hsu, C. Chang, and W. Hsieh, Fabrication and optical property of GaSe thin films grown by pulsed laser deposition, *Jpn. J. Appl. Phys.* 42(Part1(8), 5217 (2003)
31. S. R. Jian, J. Juang, C. W. Luo, S. N. Ku, and K. Wu, Nanomechanical properties of GaSe thin films deposited on Si(111) substrates by pulsed laser deposition, *J. Alloys Compd.* 542, 124 (2012)
32. S. V. Sorokin, P. S. Avdienko, I. V. Sedova, D. A. Kirilenko, M. A. Yagovkina, A. N. Smirnov, V. Y. Davydov, and S. V. Ivanov, Molecular-beam epitaxy of two-dimensional GaSe layers on GaAs(001) and GaAs(112) substrates: Structural and optical properties, *Semiconductors* 53(8), 1131 (2019)
33. X. Yuan, L. Tang, S. S. Liu, P. Wang, Z. G. Chen, C. Zhang, Y. W. Liu, W. Y. Wang, Y. C. Zou, C. Liu, N. Guo, J. Zou, P. Zhou, W. D. Hu, and F. X. Xiu, Arrayed van der Waals vertical heterostructures based on 2D GaSe grown by molecular beam epitaxy, *Nano Lett.* 15(5), 3571 (2015)

34. C. W. Liu, J. J. Dai, S. K. Wu, N. Q. Diep, S. H. Huynh, T. T. Mai, H. C. Wen, C. T. Yuan, W. C. Chou, J. L. Shen, and H. H. Luc, Substrate-induced strain in 2D layered GaSe materials grown by molecular beam epitaxy, *Sci. Rep.* 10(1), 12972 (2020)
35. K. Çınar Demir, Ş. Aydoğan, E. Gür, C. Coşkun, and Z. Aygün, Synthesis and characterization of p-GaSe thin films and the analyses of *I–V* and *C–V* measurements of p-GaSe/p-Si heterojunction under electron irradiation, *Radiat. Eff. Defects Solids* 172(7-8), 650 (2017)
36. P. Sutter, J. S. French, L. Khosravi Khorashad, C. Argyropoulos, and E. Sutter, Optoelectronics and nanophotonics of vapor-liquid-solid grown GaSe van der Waals nanoribbons, *Nano Lett.* 21(10), 4335 (2021)
37. L. Peng, Z. Xu, Z. Liu, Y. Y. Wei, H. Y. Sun, Z. Li, X. L. Zhao, and C. Gao, An iron-based green approach to 1-h production of single-layer graphene oxide, *Nat. Commun.* 6(1), 5716 (2015)
38. L. L. Tan, Q. B. Liu, Y. F. Ding, X. G. Lin, W. Hu, M. Q. Cai, and H. Zhou, Effective shape-controlled synthesis of gallium selenide nanosheets by vapor phase deposition, *Nano Res.* 13(2), 557 (2020)
39. N. Zhou, R. Y. Wang, X. Zhou, H. Y. Song, X. Xiong, Y. Ding, J. T. Lu, L. Gan, and T. Y. Zhai, P-GaSe/N-MoS_2 vertical heterostructures synthesized by van der Waals epitaxy for photoresponse modulation, *Small* 14(7), 1702731 (2018)
40. Y. B. Zhou, B. Deng, Y. Zhou, X. B. Ren, J. B. Yin, C. H. Jin, Z. F. Liu, and H. L. Peng, Low-temperature growth of two-dimensional layered chalcogenide crystals on liquid, *Nano Lett.* 16(3), 2103 (2016)
41. X. Xiong, Q. Zhang, X. Zhou, B. Jin, H. Q. Li, and T. Y. Zhai, One-step synthesis of p-type GaSe nanoribbons and their excellent performance in photodetectors and phototransistors, *J. Mater. Chem. C* 4(33), 7817 (2016)
42. X. Li, J. Dong, J. C. Idrobo, A. A. Puretzky, C. M. Rouleau, D. B. Geohegan, F. Ding, and K. Xiao, Edge-controlled growth and etching of two-dimensional GaSe monolayers, *J. Am. Chem. Soc.* 139(1), 482 (2017)
43. X. Li, M. Lin, J. Lin, B. Huang, A. A. Puretzky, C. Ma, K. Wang, W. Zhou, S. T. Pantelides, M. Chi, I. Kravchenko, J. Fowlkes, C. M. Rouleau, D. B. Geohegan, and K. Xiao, Two-dimensional GaSe-$MoSe_2$ misfit bilayer heterojunctions by van der Waals epitaxy, *Nanomaterials (Basel)* 2, e1501882 (2016)
44. G. Han, Z. G. Chen, L. Yang, L. Cheng, K. Jack, J. Drennan, and J. Zou, Thermal stability and oxidation of layer-structured rhombohedral In_3Se_4 nanostructures, *Appl. Phys. Lett.* 103(26), 263105 (2013)
45. W. J. Huang, L. Gan, H. Q. Li, Y. Ma, and T. Y. Zhai, Phase-engineered growth of ultrathin InSe flakes by chemical vapor deposition for high-efficiency second harmonic generation, *Chemistry* 24(58), 15678 (2018)
46. A. Kuhn, A. Chevy, and R. Chevalier, Crystal structure and interatomic distances in GaSe, *Phys. Status Solidi A* 31(2), 469 (1975)
47. Z. N. Guo, H. Zhang, S. B. Lu, Z. T. Wang, S. Y. Tang, J. D. Shao, Z. B. Sun, H. H. Xie, H. Y. Wang, X. F. Yu, and P. K. Chu, From black phosphorus to phosphorene: Basic solvent exfoliation, evolution of Raman scattering, and applications to ultrafast photonics, *Adv. Funct. Mater.* 25(45), 6996 (2015)
48. S. F. Quan, Y. Y. Wang, Y. Liang, J. Jiang, B. Zhong, K. Yu, H. Zhang, and G. F. Kan, Interference effect on photoluminescence intensity in GaSe up to 200 layers, *J. Phys. Chem. C* 124(18), 10185 (2020)
49. X. Zhou, J. Cheng, Y. Zhou, T. Cao, H. Hong, Z. Liao, S. Wu, H. Peng, K. Liu, and D. Yu, Strong second-harmonic generation in atomic layered GaSe, *J. Am. Chem. Soc.* 137(25), 7994 (2015)
50. L. Tang, C. Teng, Y. Luo, U. Khan, H. Pan, Z. Cai, Y. Zhao, B. Liu, and H. M. Cheng, Confined van der Waals epitaxial growth of two-dimensional large single-crystal In_2Se_3 for flexible broadband photodetectors, *Research* 2019, 2763704 (2019)
51. X. Zhou, Q. Zhang, L. Gan, H. Q. Li, and T. Y. Zhai, Large-size growth of ultrathin SnS_2 nanosheets and high performance for phototransistors, *Adv. Funct. Mater.* 26(24), 4405 (2016)
52. F. Xia, T. Mueller, Y. M. Lin, A. Valdes-Garcia, and P. Avouris, Ultrafast graphene photodetector, *Nat. Nanotechnol.* 4(12), 839 (2009)
53. J. Xia, X. Huang, L. Z. Liu, M. Wang, L. Wang, B. Huang, D. D. Zhu, J. J. Li, C. Z. Gu, and X. M. Meng, CVD synthesis of large-area, highly crystalline $MoSe_2$ atomic layers on diverse substrates and application to photodetectors, *Nanoscale* 6(15), 8949 (2014)
54. M. Hafeez, L. Gan, H. Q. Li, Y. Ma, and T. Y. Zhai, Chemical vapor deposition synthesis of ultrathin hexagonal $rese_2$ flakes for anisotropic Raman property and optoelectronic application, *Adv. Mater.* 28(37), 8296 (2016)
55. C. Y. Yan, L. Gan, X. Zhou, J. Guo, W. J. Huang, J. W. Huang, B. Jin, J. Xiong, T. Y. Zhai, and Y. R. Li, Space-confined chemical vapor deposition synthesis of ultrathin HfS_2 flakes for optoelectronic application, *Adv. Funct. Mater.* 27(39), 1702918 (2017)
56. W. J. Huang, H. Y. Hou, X. B. Chen, and T. Y. Zhai, Synthesis of superlattice InSe nanosheets with enhanced electronic and optoelectronic performance, *Chem. J. Chin. Univ.* 41(4), 682 (2020)
57. M. S. Claro, J. Grzonka, N. Nicoara, P. J. Ferreira, and S. Sadewasser, Wafer-scale fabrication of 2D β-In_2Se_3 photodetectors, *Adv. Opt. Mater.* 9(1), 2001034 (2021)
58. Y. Lu, J. Chen, T. Chen, Y. Shu, R. J. Chang, Y. Sheng, V. Shautsova, N. Mkhize, P. Holdway, H. Bhaskaran, and J. H. Warner, Controlling defects in continuous 2D GaS films for high-performance wavelength-tunable UV-discriminating photodetectors, *Adv. Mater.* 32(7), 1906958 (2020)
59. S. Lei, L. Ge, Z. Liu, S. Najmaei, G. Shi, G. You, J. Lou, R. Vajtai, and P. M. Ajayan, Synthesis and photoresponse of large GaSe atomic layers, *Nano Lett.* 13(6), 2777 (2013)